Systematic Decomposition of the Positive Bias Stress Instability in Self-Aligned Coplanar InGaZnO Thin-Film Transistors

Sungju Choi, Juntae Jang, Hara Kang, Ju Heyuck Baeck, Jong Uk Bae, Kwon-Shik Park, Soo Young Yoon, In Byeong Kang, Dong Myong Kim, *Member, IEEE*, Sung-Jin Choi, Yong-Sung Kim, Saeroonter Oh, *Member, IEEE*, and Dae Hwan Kim, *Senior Member, IEEE*

***Abstract*— We propose an experimental method to decompose the positive gate-bias stress (PBS)-induced threshold voltage shift (ΔV_{th}) of amorphous InGaZnO (a-IGZO) thin-film transistors (TFTs) into the contributions of distinct degradation mechanisms. Top-gate self-aligned coplanar structure TFTs are used for this letter. Stress-time-divided measurements, which combine the subgap density-of-states (DOS) extraction and the analysis on recovery characteristics, are performed to separate the ΔV_{th} components. Change in excess oxygen (O_{ex})-related DOS is clearly observed, and ΔV_{th} by PBS is quantitatively decomposed into the contributions of the active O_{ex}, and the deep and shallow gate insulator traps. The quantitative decomposition of PBS-induced ΔV_{th} provides physical insight and key guidelines for PBS stability optimization of a-IGZO TFTs.**

***Index Terms*— Positive bias stress (PBS), InGaZnO thin-film transistor, self-aligned coplanar structure.**

I. Introduction

AMORPHOUS metal-oxide semiconductors are used as the backplane for large-screen organic light-emitting diode (OLED) displays and liquid-crystal displays (LCDs) [1], [2], as well as flexible thin-film transistors (TFTs) fabricated on plastic substrates. Amorphous InGaZnO (a-IGZO) is a popular oxide material for its good uniformity over large areas, low processing temperatures, along with good device characteristics [3]. Current-driving TFTs in an OLED pixel, as well as TFTs in gate-driver circuitry are often under the influence of positive gate-bias stress (PBS). The physical origin of PBS instability has been classified into either 1) trapping of electrons in the gate insulator (GI), or 2) change in defect states in the active region [4]. In the former case, the electrons are trapped in border traps within the GI, or at the GI/channel interface region consisted of metal-cations, Si, and O [5], [6]. For the latter case, several explanations are given including: transition of oxygen vacancy charge states from V_O^0 to V_O^{2+}, migration of ionic defects, metal-cation interstitials, and change in a-IGZO stoichiometry [7]–[9]. In previous reports, the PBS instability has been attributed to one of the two stated mechanisms as the dominant mechanism. However, since several degradation mechanisms of different nature may take part in the PBS instability, ascribing to one particular dominant mechanism may be meaningless. Therefore, a method that can systematically dissect the PBS instability into several mechanisms is required.

In this work, we introduce a method that quantitatively decomposes the threshold voltage shift (ΔV_{th}) under the influence of PBS, into distinct degradation mechanisms. We use experimental methods that are easily applicable and do not require elaborate characterization equipment or complicated post-processing via simulation techniques. Density-of-states (DOS) extraction and stress-time-divided recovery measurements are performed to break down the separate mechanism components, and find the quantitative contribution of each component.

II. Experimental Procedure

The a-IGZO TFTs employed in this study have a top-gate self-aligned coplanar structure [1]. First, a 300-nm SiO_2 buffer layer is formed on a glass substrate by plasma-enhanced chemical vapor deposition (PECVD). Next, a 30-nm a-IGZO layer (In:Ga:Zn $=$ 1 : 1 : 1 at%) is deposited by dc sputtering. A 100-nm SiO_2 layer is deposited by PECVD to serve as the GI. Inter-layer dielectrics are deposited and patterned for source/drain (S/D) openings. Gate and S/D electrodes are formed by sputtering Cu/MoTi. Device width (W) and length (L) are 12 μm and 6 μm, respectively. PBS conditions are gate-to-source voltage (V_{GS}) of 30 V and drain-to-source voltage (V_{DS}) of 0 V, while the bias conditions for recovery are $V_{GS} = 0$ V and $V_{DS} = 0$ V, in dark conditions at room temperature. The fabricated devices have V_{th} (threshold voltage) $=$ 0.89 V, SS (subthreshold slope) $=$ 0.17 V/dec, $\mu_{FE,sat}$(saturation mobility) $=$ 10.3 cm^2/V·s, and a hysteresis of 0.017 V. The changes in SS and $\mu_{FE,sat}$ during PBS and recovery are less than 1%.

The subgap DOS is extracted by using the monochromatic photonic capacitance-voltage (MPCV) technique, where the

Manuscript received February 23, 2017; accepted March 8, 2017. Date of publication March 10, 2017; date of current version April 24, 2017. This work was supported in part by LG Display Company, in part by the National Research Foundation of Korea through the Korean Government (MSIP) under Grant 2016R1A5A1012966 and Grant 2015M3D1A1068061, in part by SILVACO, and in part by the IC Design Education Center. The review of this letter was arranged by Editor W. S. Wong. *(Corresponding authors: Saeroonter Oh; Dae Hwan Kim.)*

S. Choi, J. Jang, H. Kang, D. M. Kim, S.-J. Choi, and D. H. Kim are with the School of Electrical Engineering, Kookmin University, Seoul 02707, South Korea (e-mail: drlife@kookmin.ac.kr).

J. H. Baeck, J. U. Bae, K.-S. Park, S. Y. Yoon, and I. B. Kang are with the Research and Development Center, LG Display Company, Paju 413-811, South Korea.

Y.-S. Kim is with the Korea Research Institute of Standards and Science, Daejeon 34113, South Korea.

S. Oh is with the Division of Electrical Engineering, Hanyang University, Ansan 15588, South Korea (e-mail: sroonter@hanyang.ac.kr).

Color versions of one or more of the figures in this letter are available online at http://ieeexplore.ieee.org.

Digital Object Identifier 10.1109/LED.2017.2681204

0741-3106 © 2017 IEEE. Personal use is permitted, but republication/redistribution requires IEEE permission.
See http://www.ieee.org/publications_standards/publications/rights/index.html for more information.

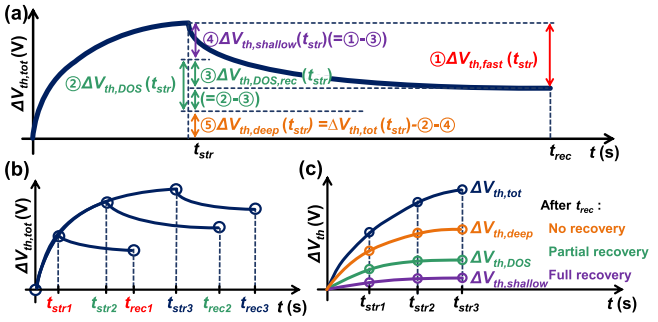

Fig. 1. (a) Decomposition of $\Delta V_{th,tot}$ at a specific t_{str} and t_{rec}. (b) Stress-time-divided measurements to obtain $\Delta V_{th,DOS}$, $\Delta V_{th,shallow}$, and $\Delta V_{th,deep}$ as functions of t_{str}. (c) Final decomposition of ΔV_{th} under PBS into three separate degradation mechanisms ($\Delta V_{th,tot} = \Delta V_{th,DOS} + \Delta V_{th,shallow} + \Delta V_{th,deep}$).

detailed methodology is given in [10]. Capacitance was measured by a LCR meter (HP4284A) using a 100 kHz ac signal. A 5 mW illumination source with a wavelength corresponding to photonic energy of 2.8 eV is used. The energy distribution of the DOS profile is obtained from V_{GS}-dependent capacitance data [10], and verified by self-consistent numerical simulations.

III. Results and Discussions

The total ΔV_{th} under PBS ($\Delta V_{th,tot}(t) = V_{th}(t) - V_{th}(t = 0)$) is a combination of several components with different nature, and is broken down by experimental techniques ($\Delta V_{th,tot}(t) = \Delta V_{th1}(t) + \Delta V_{th2}(t) + \ldots$). Fig. 1 illustrates the decomposition scheme of $\Delta V_{th,tot}(t)$ into the contributions of distinct mechanisms. After a specific stress time (t_{str}), bias conditions are switched to a recovery stage. During recovery, the ΔV_{th} lowers and saturates to a certain value. We define this recovery component as $\Delta V_{th,fast} = \Delta V_{th}(t = t_{str}) - \Delta V_{th}(t = t_{rec})$, denoted as ① in Fig. 1(a), where the recovery time t_{rec} is defined as the time when $|d\Delta V_{th,tot}/dt|$ becomes lower than 10^{-6} V/s.

Two stress-time-divided measurement techniques are used to determine the discrete degradation components. First, we extract the subgap DOS of the channel layer at t_{str} to find the PBS-induced change in DOS. The ΔV_{th} portion caused by the DOS change ($\Delta V_{th,DOS}$) is denoted as ② in Fig. 1(a). Second, ΔV_{th} recovery characteristics are probed at various stress times in between stress-time intervals, denoted by t_{str1}, t_{str2}, and t_{str3} in Fig. 1(b). In this way, $\Delta V_{th,fast}$ is sampled at $t = t_{str1}$, t_{str2}, and t_{str3} to trace the PBS time-evolution of $\Delta V_{th,fast}$.

The symbols in Fig. 2(a) and (b) show the extracted DOS profiles at $t_{str} = 0$ s (initial), $t_{str} = 10^4$ s (stress), and $t_{rec} = t_{str} + 10^4$ s (recovery). The measured DOS's are divided into four components according to their distribution shapes in energy level: donor-like tail states (g_{TD}), excess oxygen defect states (g_{Oex}), acceptor-like deep states (g_{DA}) and tail states (g_{TA}), in increasing order of the energy levels. We model the extracted DOS near E_V and E_C as:

$$g_{TD}(E) + g_{Oex}(E) = N_{TD}\exp\left(-\frac{E - E_V}{kT_{TD}}\right) + N_{Oex}\exp\left(-\left(\frac{E - E_V - E_{Oex}}{kT_{Oex}}\right)^2\right), \quad (1)$$

TABLE I
Extracted DOS Parameters at Selected Times: Initial, After 10^4 s of Stress, and After Additional 10^4 s of Recovery

Parameter		N_{dos} (eV^{-1} cm^{-3})	kT_{dos} (eV)	E_{dos} (eV)
Acceptor-like tail states, g_{TA}		2.0×10^{18}	0.03	-
Acceptor-like deep states, g_{DA}		6.0×10^{16}	0.75	0.8
Excess oxygen states, g_{Oex}	Initial	0.3×10^{16}	0.4	0.7
	After stress	0.8×10^{16}		
	After recovery	0.65×10^{16}		
Donor-like tail states, g_{TD}		5.0×10^{18}	0.015	-

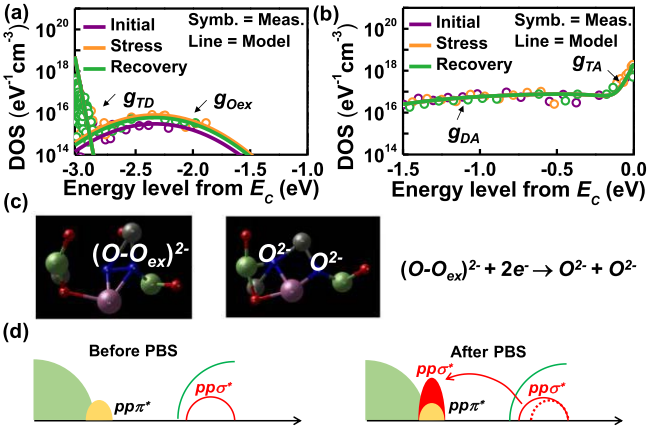

Fig. 2. Representative DOS profiles near the (a) valence band edge E_V and (b) conduction band edge E_C, extracted at three different stages: before PBS, after PBS, and after recovery. The bandgap of IGZO is measured to be 3.03 eV. Schematic diagrams illustrating (c) the microscopic origin of $\Delta V_{th,DOS}$ and (d) the increase of g_{Oex} due to PBS.

$$g_{TA}(E) + g_{DA}(E) = N_{TA}\exp\left(-\frac{E_C - E}{kT_{TA}}\right) + N_{DA}\exp\left(-\left(\frac{E_C - E_{DA} - E}{kT_{DA}}\right)^2\right), \quad (2)$$

respectively, which is denoted by the lines in Fig. 2(a) and (b). Table I shows the extracted DOS parameters, which are validated by inputting the fitted DOS parameters into a numerical device simulator, and comparing the simulated $I - V$ characteristics with experiment [11], [12]. The measured $I - V$ is well reproduced by the simulations using the experimentally extracted DOS parameters (data not shown).

Among the DOS components, g_{TD}, possibly originating from the O p-like (occupied) valance band edge or tail states in the a-IGZO, did not change significantly during PBS and recovery. g_{TA} may come from the In disorder in a-IGZO, while the origin of g_{DA} is still unknown. In our measurements, both g_{TA} and g_{DA} did not change during PBS and recovery. The prominent change in DOS is found to be the g_{Oex} component, which is located ~1 eV above the valence band edge (E_V), as shown in Fig. 2(a). g_{Oex} partially relate with the $pp\pi^*$ (occupied) states in the O_{ex} (excess oxygen) peroxide (i.e., O-O dimer) configuration, and also with the $pp\sigma^*$ states after electron-capture by the peroxide [13], [14]. During PBS,

the empty $pp\sigma^*$ anti-bonding state in the conduction bands captures two electrons letting the peroxide transform into the fully-oxidized state, i.e., $(\text{O-O}_{ex})^{2-} + 2e^- \rightarrow O^{2-} + O^{2-}$, as seen in Fig. 2(c) [13]. The occupied $pp\sigma^*$ state is then located in the g_{Oex} energy range as illustrated in Fig. 2(d) [15]. Thus, the actual change of the g_{Oex} originates from the increase of the $pp\sigma^*$ state capturing electrons, and that is the reason why g_{Oex} has an acceptor-like character and becomes the origin of positive ΔV_{th}. The increase of g_{Oex} should accompany the decrease of empty $pp\sigma^*$ states inside the conduction band. We express $\Delta V_{th,DOS}$ due to the increase of g_{Oex} after t_{str} as:

$$\Delta V_{th,DOS}(t_{str}) = \frac{qt_{act}}{C_{ox}} \left(\int_{E_V}^{E_C} g_A(E, t = t_{str})\, dE - \int_{E_V}^{E_C} g_A(E, t = 0)\, dE \right) \quad (3)$$

where q is the elementary charge of an electron, t_{act} is the active layer thickness, and C_{ox} is the gate insulator capacitance per unit area. Noticeably, the increase of g_{Oex} during PBS is found to decrease (partially recover) during additional recovery time, as shown in Fig. 2(a). Recovery of V_{th} due to the DOS restoration, $\Delta V_{th,DOS,rec}$, which is denoted by ③ in Fig. 1(a), can also be derived similarly to Eq. (3), by performing DOS integration as:

$$\Delta V_{th,DOS,rec}(t_{str}) = \frac{qt_{act}}{C_{ox}} \left(\int_{E_V}^{E_C} g_A(E, t = t_{str})\, dE - \int_{E_V}^{E_C} g_A(E,\ t = t_{rec})\, dE \right). \quad (4)$$

Hence, part of $\Delta V_{th,fast}$ should come from $\Delta V_{th,DOS,rec}$. By excluding $\Delta V_{th,DOS,rec}$ from $\Delta V_{th,fast}$, we can determine the fast recovery component caused solely by the GI, denoted by $\Delta V_{th,shallow}$ (④ in Fig. 1(a)). For now, we will attribute this self-recoverable term to electrons de-trapping from "shallow traps" in the GI or the a-IGZO/GI interface, since the electrons are able to escape the energy barrier by mere kT energy.

After disclosure of these two mechanisms, we are left with the remaining V_{th} amount that does not recover in the presence of thermal energy available at room temperature, nor originate from the DOS change in the active region. Hence, the remaining ΔV_{th} portion is most likely related with GI traps further from the interface with a higher energy barrier for de-trapping [16], [17]. Hence, we will assign the last component as "deep GI trapping" ($\Delta V_{th,deep}$: ⑤ in Fig. 1(a)), which is obtained by:

$$\Delta V_{th,deep}(t) = \Delta V_{th,tot}(t) - \Delta V_{th,DOS}(t) - \Delta V_{th,shallow}(t) \quad (5)$$

where $\Delta V_{th,tot}$ is the total ΔV_{th}, while $\Delta V_{th,DOS}$ and $\Delta V_{th,shallow}$ are the ΔV_{th} originating from DOS change in the channel (the first stress-time-divided technique), and ΔV_{th} due to shallow GI trapping (the second stress-time-divided technique), respectively. The decomposed $\Delta V_{th,DOS}$, $\Delta V_{th,shallow}$, and $\Delta V_{th,deep}$ are plotted as a function of the stress time in Fig. 1(c).

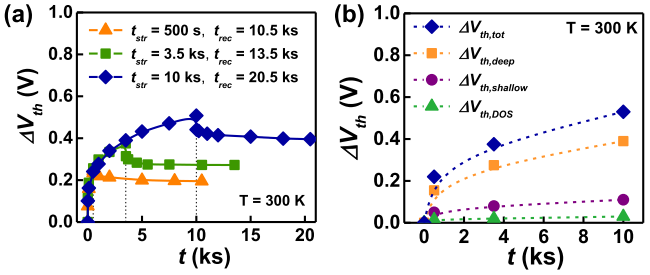

Fig. 3. (a) Decomposition of $\Delta V_{th,tot}$ using stress-time-divided measurements at t_{str} = 500 s, 3,500 s, and 10,000 s, and respective t_{rec} required for each t_{str}. (b) Final decomposition of $\Delta V_{th,tot}$ into three degradation mechanisms, with each mechanism having its own dependence on stress time.

TABLE II
DECOMPOSITION OF ΔV_{th} AT PBS TIMES OF 500, 3500, AND 10^4 s

	t_{str} = 500 s	t_{str} = 3500 s	t_{str} = 10,000 s
$\Delta V_{th,tot}$ (V)	0.22	0.375	0.53
$\Delta V_{th,DOS}$ (V)	0.015	0.02	0.03
$\Delta V_{th,shallow}$ (V)	0.05	0.08	0.11
$\Delta V_{th,deep}$ (V)	0.13	0.275	0.39
$\Delta V_{th,DOS,rec}$ (V)	0.01	0.02	0.02

Fig. 3 and Table II summarizes the PBS ΔV_{th} separation of self-aligned coplanar a-IGZO TFTs using the stress-time-divided techniques at three different stress times: 500, 3500, and 10^4 s. For the devices in this work, process conditions were controlled to minimize excess oxygen content in the GI/channel interface to reduce both $\Delta V_{th,DOS}$ and $\Delta V_{th,shallow}$, leaving the GI deep trapping component as the dominant PBTS degradation mechanism, as can be seen in Fig. 3. By utilizing the proposed method, optimization of the GI quality to getter the deep traps is suggested for further PBTS stability improvement. The quantitative decomposition of PBTS ΔV_{th} enables an effective assessment of the complex degradation nature, along with guidelines for process optimization efforts towards ultimate PBTS stability. Particularly, joint optimization of the dielectrics, the active layer, and the interfaces must be carried out to enhance stability of a-IGZO TFTs to its limits. Moving forward to other high-mobility metal-oxide materials, systematic decomposition of the degradation mechanisms followed by theoretical study and quantitative modeling will become essential for physical understanding and enhancement of device stability.

IV. CONCLUSION

In summary, we have proposed a method to experimentally identify various PBS degradation components. Stress-time-divided measurements of subgap DOS and recovery characteristics at various stress intervals were used to break down and classify the PBS instability into three distinct components: 1) increase of DOS due to excess oxygen (occupied $pp\sigma^*$ state) in the active region, 2) shallow and 3) deep charge trapping in the GI. Systematic decomposition of the degradation mechanisms provides insight into a complex system of multiple physical processes occurring simultaneously, and can be easily applied universally to any device with any stress conditions.

REFERENCES

[1] C. Ha, H. Lee, J. Kwon, S. Seok, C. K. Ryoo Yun, B. Kim, W. Shin, and S. Cha, "Self-aligned coplanar structure for large-sized ultrahigh-definition OLED TV," in *SID Int. Symp. Dig. Tech. Paper*, vol. 46. 2015, pp. 1020–1022, doi: 10.1002/sdtp.10346.

[2] B. Yeh and C. Lin, "High-performance 4K x 2K 65-in. TV with BCE-type oxide TFTs," in *SID Int. Symp. Dig. Tech. Paper*, vol. 46. 2015, pp. 943–945, doi: 10.1002/sdtp.10419.

[3] T. Kamiya, K. Nomura, and H. Hosono, "Present status of amorphous In–Ga–Zn–O thin-film transistors," *Sci. Technol. Adv. Mater.*, vol. 11, no. 4, p. 044305, 2010, doi: 10.1088/1468-6996/11/4/044305.

[4] M. J. Powell, "The physics of amorphous-silicon thin-film transistors," *IEEE Trans. Electron Devices*, vol. 36, no. 12, pp. 2753–2763, Dec. 1989.

[5] M. E. Lopes, H. L. Gomes, M. C. R. Medeiros, P. Barquinha, L. Pereira, E. Fortunato, R. Martins, and I. Ferreira, "Gate-bias stress in amorphous oxide semiconductors thin-film transistors," *Appl. Phys. Lett.*, vol. 95, no. 6, p. 063502, 2009, doi: 10.1063/1.3187532.

[6] S. Oh, J. H. Baeck, J. U. Bae, K.-S. Park, and I. B. Kang, "Effect of interfacial excess oxygen on positive-bias temperature stress instability of self-aligned coplanar InGaZnO thin-film transistors," *Appl. Phys. Lett.*, vol. 108, no. 14, p. 141604, 2016, doi: 10.1063/1.4945404.

[7] A. Janotti and C. Van de Walle, "Native point defects in ZnO," *Phys. Rev. B, Condens. Matter*, vol. 76, no. 16, pp. 165202-1–165202-22, Oct. 2007, doi: http://dx.doi.org/10.1103/PhysRevB.76.165202.

[8] A. J. Flewitt and M. J. Powell, "A thermalization energy analysis of the threshold voltage shift in amorphous indium gallium zinc oxide thin film transistors under simultaneous negative gate bias and illumination," *J. Appl. Phys.*, vol. 115, no. 13, p. 134501, 2014, doi: 10.1063/1.4870457.

[9] H.-H. Nahm and Y.-S. Kim, "Undercoordinated indium as an intrinsic electron-trap center in amorphous $InGaZnO_4$," *NPG Asia Mat.*, vol. 6, p. e143, Nov. 2014, doi: 10.1038/am.2014.103.

[10] H. Bae, H. Choi, S. Jun, C. Jo, Y. H. Kim, J. S. Hwang, J. Ahn, S. Oh, J. U. Bae, S.-J. Choi, D. H. Kim, and D. M. Kim, "Single-scan monochromatic photonic capacitance-voltage technique for extraction of subgap DOS Over the bandgap in amorphous semiconductor TFTs," *IEEE Electron Device Lett.*, vol. 34, no. 12, pp. 1524–1526, Dec. 2013, doi: 10.1109/LED.2013.2287511.

[11] T. Kamiya, K. Nomura, and H. Hosono, "Present status of amorphous In-Ga-Zn-O thin-film transistors," *Sci. Technol. Adv. Mater.*, vol. 11, no. 4, p. 44305, Aug. 2010, doi: 10.1088/1468-6996/11/4/044305.

[12] E. K.-H. Yu, S. Jun, D. H. Kim, and J. Kanicki, "Density of states of amorphous In-Ga-Zn-O from electrical and optical characterization," *J. Appl. Phys.*, vol. 116, no. 15, p. 154505, 2014.

[13] W. H. Han, Y. J. Oh, K. J. Chang, and J.-S. Park, "Electronic structure of oxygen interstitial defects in amorphous In-Ga-Zn-O semiconductors and implications for device behavior," *Phys. Rev. Appl.*, vol. 3, no. 4, p. 044008, 2015, doi: 10.1103/PhysRevApplied.3.044008.

[14] H.-H. Nahm, Y.-S. Kim, and D. H. Kim, "Instability of amorphous oxide semiconductors via carrier-mediated structural transition between disorder and peroxide state," *Phys. Status Solidi B*, vol. 249, no. 6, pp. 1277–1281, 2012.

[15] K. Ide, Y. Kikuchi, K. Nomura, M. Kimura, T. Kamiya, and H. Hosono, "Effects of excess oxygen on operation characteristics of amorphous In-Ga-Zn-O thin-film transistors," *Appl. Phys. Lett.*, vol. 99, no. 9, p. 093507, Sep. 2011.

[16] H. Kakhdari, D. Vuillaume, and J. C. Bourgoin, "Spatial and energetic distribution of Si-SiO_2 near-interface states," *Phys. Rev. B, Condens. Matter*, vol. 38, no. 18, pp. 13124–13132, 1988, doi: 10.1103/PhysRevB.38.13124.

[17] E. P. Gusev and C. P. D'Emic, "Charge detrapping in HfO_2 high-k gate dielectric stacks," *Appl. Phys. Lett.*, vol. 83, no. 25, pp. 5223–5225, Dec. 2003, doi: 10.1063/1.1633332.